PROCEEDINGS OF MOSES2023 CONFERENCE
4TH INTERNATIONAL CONFERENCE ON MODELLING AND OPTIMISATION OF SHIP ENERGY SYSTEMS
26-27 OCTOBER 2023, DELFT, NETHERLANDS

Equivalent Consumption Minimization Strategy for Full-Electric Ship Energy Management with Multiple Objectives

Charlotte Löffler[a*], Rinze Geertsma[b], Despoina Mitropoulou[c], Henk Polinder[a], and Andrea Coraddu[a]

[a]Delft University of Technology, Delft, Netherlands
[b]Netherlands Defense Academy, Den Helder, Netherlands
[c]RH Marine, Schiedam, Netherlands
[*]c.loeffler@tudelft.nl

Abstract

Optimal energy management is still a challenge in full-electric vessels. New degrees of flexibility in the energy management resulting from the load sharing between multiple, heterogenous power sources lead to a suboptimal solution using rule-based control. Therefore, advanced control strategies present a solution to the challenge of finding the optimal control input for a nonlinear multi-objective power and energy problem in sufficient time. As additional benefit, advanced control allows to incorporate multiple objectives in the optimization such as minimization of several emissions, operational costs, and component degradation. Equivalent Consumption Minimization Strategy (ECMS) is a strategy for instantaneous optimization, which is promising for applications in vessels with a high degree of uncertainty in the load profile. It incorporates multiple objectives by assigning equivalent cost factors in the cost function, allowing a flexible expansion of the control problem. In this paper, we present a novel ECMS-based control strategy for a full-electric vessel with the ability to react flexibly to changing mission conditions. First, we define the objectives for the control problem, in this study CO_2 production, hazardous emission production, fuel consumption, energy cost, and the degradation of the battery. Second, we develop a pareto-front approach for a-posteriori definition of the equivalent cost factors. To showcase energy consumption reduction, we use a benchmark control based on state-of-the-art control strategies. A full-electric case study vessel with high uncertainty in the load profile is chosen to evaluate the proposed controller. Several different load profiles are generated and tested to evaluate the performance of the ECMS controller in dealing with different types of loads. The results will demonstrate the effectiveness of the proposed novel control strategy in reducing energy consumption while minimizing other hazardous emission outputs and preserving the health of the battery.

Keywords: Energy Management; Full-Electric Vessel; ECMS; Multiobjective Optimization; NOx emission.

1 INTRODUCTION

The electrification of vessels is an important step in the direction of climate-friendly transportation [1]. Full-electric vessels often combine heterogeneous power generation and storage components, which allows for a more fuel-efficient operation and decreased CO_2 emission [2]. However, this enhanced flexibility of the power generation also leads to a raised complexity of the system [3]. This raised system complexity leads to a non-optimal control solution using rule-based control (RBC) [4]. A solution to this problem is to use advanced control strategies. An additional benefit of advanced control is the possibility to minimize several objectives alongside the control strategy.

The first step to change the propulsion system of a vessel towards zero-emission is to use battery-only systems [5]. However, the short autonomous travel distance limits the application of battery-only systems due to the relatively low energy density of batteries [6]. The autonomous travel distance can be increased by using alternative fuels in the propulsion system [5]. Alternative fuels can be used in a variety of technologies such as Internal Combustion Engines (ICE) or fuel cells (FC) [7]. The first step to introduce alternative fuels in the energy management of a full-electric vessel is the operation of different sets of diesel engines alongside to benefit from their individual characteristics. One major benefit of using ICE is the ability to provide high loads with comparatively fast dynamic response at low cost [8].

However, ICE still produce emission under operation. One emission, which is not often considered in current control research in the maritime is the production of NOx. Different than CO_2 output, which relates linear to the fuel consumption, the formation of NOx is not correlated to the fuel consumption but rather to the operational conditions in the en-

DOI: https://doi.org/10.59490/moses.2023.673

gine. Considering this in a control problem adds to the complexity of the developed control since several more objectives are relevant to vessel energy management. While another major cost factor for the control is the reduction of fuel consumption, the extension of components' lifetime due to optimal usage gains more interest with full-electric systems operating with batteries and fuel cells. This combination of several objectives in the same strategy is called multi-objective control. All the objectives of interest for the vessel control can be categorized into different categories. Depending on the type of objective, the optimal point of operation differs, so the control has to find the best possible compromise. Batteries introduce greater flexibility into the operation of energy systems. However, their degradation, influenced by time and improper usage, cannot be overlooked. This degradation leads to increased maintenance and replacement costs. One major problem of multi-objective control is that it expands the control problem further, leading to raised algorithm solution times.

Current approaches on multi-objective control mainly combine fuel consumption and CO_2 emission reduction [9]–[12]. Research also started to address the combination of fuel cost reduction with an extension of the battery lifetime [13]–[15]. The combination of objectives from more than two categories, such as fuel cost, emission production, and degradation, is rarely investigated [12], [15], [16]. However, even those only focus on the CO_2 production as emission output. The incorporation of emission production besides CO_2 ensures the protection of sensitive areas by specific optimization. For a holistic optimization of the operation, the aspects of battery degradation and fuel price have to be combined with the emission reduction.

One promising advanced control strategy, which is able to optimize between several objectives quickly, is Equivalent Consumption Minimization (ECMS). A main advantage of ECMS is the instantaneous optimization in one step, which makes it suitable for high degrees of uncertainty and fast dynamics. ECMS was already studied for its application in the automotive sector, where it is used to keep up with the quick dynamics in real-time [17]. For maritime application, Kalikatzarakis et al. [18] applied it for the reduction of fuel consumption, which showed promising first results. Even though the authors successfully apply ECMS to a marine energy management problem, the strategy's potential to minimise more than one objective needs further investigation.

2 PROPULSION LAYOUT

A full-electric vessel of the type Yacht is selected as the case for this paper. The vessel is operating with a DC-distribution system with two directly connected battery packs as energy storage system. The power generation uses two pairs of diesel generators of different sizes. The generator sets are connected via AC/DC converters to the DC grid, which allows for a variable speed operation of the engines.

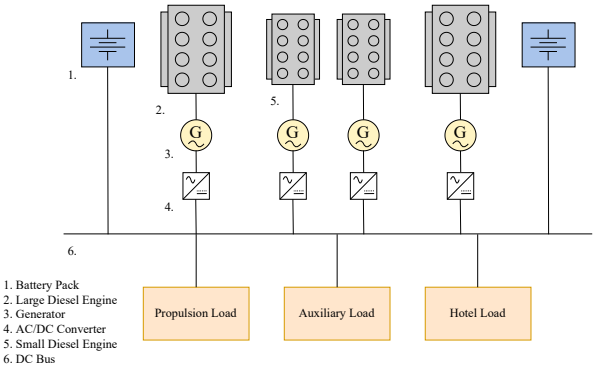

Figure 1: Propulsive layout of the usecase vessel

2.1 System Modelling

We model the behavior of the propulsion system using steady-state, first-principle equations. These models are derived from mathematical relationships combined with empirical measurements of the components. In the table below are the specifications of the propulsion system summarized. In the following, we introduce the models used to describe the component behaviour.

Table 1: Case study parameters

Parameter	Description	Value
V_{DC}	DC-bus voltage	$800 - 1000\,\mathrm{V}$
$P_{E,l}$	Engine power (x2)	$1430\,\mathrm{KWe}$
$P_{E,s}$	Engine power (x2)	$895\,\mathrm{KWe}$
E_{Bat}	Battery capacity (x2)	$2250\,\mathrm{KWh}$
η_{AC-DC}	Conversion efficiency	0.98
η_{DC-AC}	Conversion efficiency	0.98
η_{DC-DC}	Conversion efficiency	0.98
η_m	Motor efficiency	0.97
η_{gb}	Gearbox loss	0.97
η_{gen}	Generator efficiency	0.96

For the battery packs, we use the research of Tremblay et al. [19] for a generic battery model of a Lithium-Ion battery. The battery model is scaled to match the required size for the vessel battery packs. The control of the battery is indirect over the control of the engines using the power balance of the

system. No individual set point is required as the batteries are connected directly to the DC bus.

The system contains two sets of two combinations of engine and generator for the propulsion, which all operate using Diesel. We model the engines using performance maps, which are created over the engine's operating envelope. Since we combine the engines with a DC grid in this study, the engines can be operated flexibly using variable speed set points. For each type of engine, the specific fuel consumption (SFC) is mapped over speed in rounds per minute [rpm] and power [kWh]. The emission production is modelled in two different ways: while the CO_2 production can be related linearly to the SFC, the NOx formation is related to the engine's operational conditions and not the SFC. We model the NOx emission by creating a similar map over the operational envelope based on real-world measurements. The engines are controlled with a set point for the requested power and one for the speed.

The other power system components are modelled using transfer functions for the losses. This includes the gear box, generators, electrical motors, converters, and the DC grid. The selected values are derived from information provided by the shipbuilder and manufacturers; however, we cannot disclose the specific values due to confidentiality reasons.

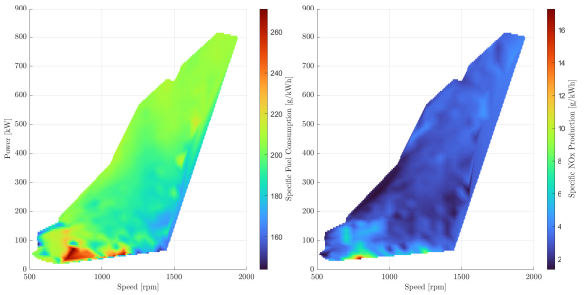

Figure 2: SFC and NOX maps for small engine [20]

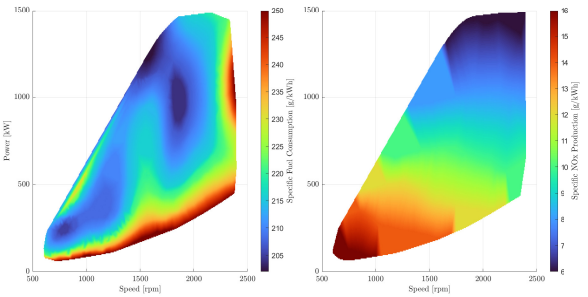

Figure 3: SFC and NOX maps for large engine [21]

3 CONTROL DEVELOPMENT

For the energy management of the vessel, a 2-level multi-objective ECMS controller is developed. While the first layer decides the optimal power scheduling combination of components, the second layer determines the optimal set points for the components in use. The controller uses a set of variables to describe the system's behaviour. The system is defined by four states: the engine current (I_{Eng}), the load current (I_{Load}), the battery current (I_{Bat}) as represented in the power balance on the DC bus, and the state of charge (SoC_{Bat}) for one of the battery packs. For clarity, these states are denoted as $I_{\text{Eng}} = x_1$, $I_{\text{Load}} = x_2$, $I_{\text{Bat}} = x_3$, and $SoC_{\text{Bat}} = x_4$. Additionally, there are eight control variables: four related to engine power ($P_{\text{Eng,i}} = u_i$ for $i \in 1,2,3,4$) and four to engine speed ($n_{\text{Eng,i}} = u_j$ for $j \in 5,6,7,8$). A comprehensive overview of these state and control variables, along with other inputs and parameters, is provided in Table 2.

Table 2: State and Control Variables, Input, and Parameters

Parameter	Description	Role
I_{Eng}	Engine Current	State
I_{Load}	Requested Load Current	State
I_{Bat}	Battery Current	State
SoC_{Bat}	Battery State of Charge	State
$P_{\text{Eng,i}}$	i^{th} Engine Power Reference	Control
$n_{\text{Eng,i}}$	i^{th} Speed Reference	Control
P_{Prop}	Propulsion Load	Input
P_{Aux}	Auxiliary Load	Input
V_{DC}	DC Voltage	Input
r_{CO2}	Release Rate CO_2	Const.
p_{D}	Price of diesel	Const.
p_{Bat}	Equivalent factor battery	Const.
n_{p}	Battery modules in parallel	Const.
Q_{nom}	Battery nominal power	Const.

It is worth noting that only one battery pack is considered since both behave identically due to the direct connection to the DC bus. The four states are shown in Eq. 1.

$$
\begin{aligned}
x_1 &= \frac{(u_1 + u_2 + u_3 + u_4) \cdot \eta_{gen}}{V_{\text{DC}}} \cdot \eta_{\text{AC-DC}} \\
x_2 &= \frac{P_{\text{Prop}} \cdot 1/\eta_{gb} \cdot 1/\eta_m + P_{\text{Aux}}}{V_{\text{DC}} \cdot \eta_{\text{DC-AC}}} \\
x_3 &= x_1 - x_2 \\
x_4 &= x_{4n-1} + \frac{1}{2} \frac{\Delta t \cdot x_3}{Q_{\text{nom}} \cdot n_p}
\end{aligned}
\tag{1}
$$

Using the relationships outlined in Eq. 1, the ref-

erences for the state variables can be determined, which must be matched by the controller's states to ensure the similarity to the real system. In addition, a set of objectives is defined to optimize special targets. First, the control variables of the problem are used to determine the SFC and the NOx production of the engines based on the maps in Fig. 2 and Fig. 3. With $i \in \{1, 2\}$ and $j \in \{3, 4\}$, the SFC and NOx of the engines 1-4 can be expressed as

$$\mathrm{SFC}_{\mathrm{Eng,i}} = f_1(u_i, u_{i+4}) \tag{2}$$
$$\mathrm{NOx}_{\mathrm{Eng,i}} = f_2(u_i, u_{i+4}) \tag{3}$$
$$\mathrm{SFC}_{\mathrm{Eng,j}} = f_3(u_j, u_{j+4}) \tag{4}$$
$$\mathrm{NOx}_{\mathrm{Eng,j}} = f_4(u_j, u_{j+4}) \tag{5}$$

where f_1 and f_2 are functions that represent the SFC and NOx formation of the small engines, and f_3 and f_4 are similar functions for the large engines. Using those references, we calculate the mass of fuel consumed (m_{D}) and emission produced ($m_{\mathrm{CO_2}}, m_{\mathrm{NOx}}$) as

$$m_{\mathrm{D}} = \sum_{i=1}^{4} \mathrm{SFC}_{\mathrm{Eng,i}} \cdot u_i \tag{6}$$
$$m_{\mathrm{CO_2}} = \sum_{i=1}^{4} \mathrm{SFC}_{\mathrm{Eng,i}} \cdot u_i \cdot r_{\mathrm{CO2}} \tag{7}$$
$$m_{\mathrm{NOx}} = \sum_{i=1}^{4} \mathrm{NOx}_{\mathrm{Eng,i}} \cdot u_i \tag{8}$$

where $r_{\mathrm{CO_2}}$ is the release rate of CO_2 from diesel during combustion.

3.1 Objective Function Definition

We introduce three objectives to account for the fuel consumption and emission production in the objective function. While the first objective C_1 represents the price of a kWh as a comparison between the engines and the batteries, the latter objectives C_2 and C_3 account for the mass of emission formatted under operation. The price of a kWh diesel is related to a pricing factor p_{D} representing the fuel's market value. To allow for comparison, an equivalent pricing factor for the battery p_{Bat} is defined. With this, the three objectives are set up as denoted in Eq. 9.

$$\begin{aligned} \mathrm{C}_1 &: m_{\mathrm{D}} \cdot p_{\mathrm{D}} + P_{\mathrm{Bat}} \cdot p_{\mathrm{Bat}} \\ \mathrm{C}_2 &: m_{\mathrm{CO_2}} \\ \mathrm{C}_3 &: m_{\mathrm{NOx}} \end{aligned} \tag{9}$$

The objectives are normalized to allow an equal comparison of the differently-natured targets.

We account for the battery's health by imposing constraints on the minimum and maximum of the SOC. Those boundaries ensure the operation to stay between 20% and 80% SOC. Further, we aim to avoid excessive battery currents by introducing a penalty for the depth of discharge (DoD) using a penalty factor c_{Bat}. This penalty term is $c_{\mathrm{Bat}} \cdot (x_4 - 0.5)$.

The three objectives are incorporated in a scalarized objective function function. Each of those objectives is combined with a weight λ_i with the index $i \in \{1, 2, 3\}$. This leads to

$$J(\mathbf{x}, \mathbf{u}) = \sum \lambda_i \cdot \mathrm{C}_i, \tag{10}$$

where $\mathbf{x}$ and $\mathbf{u}$ represent the state and control variables, as reported in Tab. 2.

3.2 Optimization Problem

We solve the multi-objective optimization problem to determine the optimal control input for the vessel energy system. For this purpose, the objective function, represented in Eq. 10, is expanded with two parts. The first one includes the controller's reference values of the state variables in the form of $\mathbf{x}_{\mathrm{ref}}$, which penalizes a deviation from the expected values of the real system. The second one adds the penalty for the depth of discharge DoD. Taking this into account, the final objective function can be expressed as:

$$J(\mathbf{x}, \mathbf{u}) = (\mathbf{x} - \mathbf{x}_{\mathrm{ref}}) + \mathrm{DoD} + \sum \lambda_i \cdot \mathrm{C}_i, \tag{11}$$

Additionally, constraints are imposed to further characterize the minimization problem. The first prominent constraint is the power balance between the requested and the generated power in the form of

$$P_{\mathrm{Load}} = P_{\mathrm{Gen}}. \tag{12}$$

Further constraints limit the operational range of system components as following

$$\mathcal{O}_{\mathrm{lower}} \leq \mathcal{O} \leq \mathcal{O}_{\mathrm{upper}}, \tag{13}$$

where $\mathcal{O}$ stands for the component with its respective lower $\mathcal{O}_{\mathrm{lower}}$ and upper $\mathcal{O}_{\mathrm{upper}}$ limits. The upper and lower limits of the two types of engines are characterized by non-linear functions describing the respective threshold. Therefore, the Eq. 13 for the constraints imposed on the engines are represented for $i \in \{1, 2, 3, 4\}$:

$$f_{\mathrm{lower,i}}(\mathbf{x}) \leq \mathcal{O}_{\mathrm{Eng,i}} \leq f_{\mathrm{upper,i}}(\mathbf{x}), \tag{14}$$

5 where $\mathcal{O}_{\mathrm{Eng,i}}$ stands for the i-th engine and $f_{\mathrm{lower,i}}(\mathbf{x})$ and $f_{\mathrm{upper,i}}(\mathbf{x})$ are the corresponding non-linear functions of the lower and upper limit.

Based on those constraints and our knowledge about the system behavior, we aim to identify the set of optimal control inputs $\mathbf{u}(\cdot|k)_{\text{opt}}$ that minimizes the objective function J, respective Eq. 11. This leads to the following minimization problem:

$$\begin{aligned} \text{Minimize:} \quad & J(\mathbf{u}(\cdot|k)) \\ \text{s.t.:} \quad & \\ & \mathbf{x}_{k+1} = f(\mathbf{x}_k, \mathbf{u}_k) \\ & \mathbf{u}_k = \mathbf{u}_{k-1} + \Delta\mathbf{u}_k \\ & g_{\text{in}}(\mathbf{x}_k, \mathbf{u}_k) \leq 0 \\ & g_{\text{eq}}(\mathbf{x}_k, \mathbf{u}_k) = 0 \end{aligned} \tag{15}$$

where $\mathbf{x}_{k+1}$ corresponds to the state at the next time step as a function of the current values of the state variables x_k and the control variables u_k. The value of the control u_k in time step k is formed by adding the difference in the control value $\Delta\mathbf{u}_k$ to the control value u_{k-1} of time step $k-1$. The equality and inequality constraints set is represented by g_{eq} and g_{in} in dependence on the control and state variables u_k and x_k.

Eq. 15 analysis shows the problem to be nonlinear and non-convex in combination with nonlinear constraints. A problem natured like this can be solved by applying different approaches [22]. According to Wolpert et Macready [23] and their no free lunch theorem, determining the optimal algorithm for an optimization problem a-priori is impossible. This decision is only possible by testing various ones and later comparing their performance. However, in this study, we decide to apply Sequential Quadratic Programming (SQP) [24], as it includes the required capabilities to solve problems of the nature of Eq. 15 [25]. This is based on the works and findings of [26] and [25]. To ensure algorithm convergence and finding the global minimum, we apply a multi-start approach [27]. In concrete, we define a set of 50 randomly distributed starting points inside the defined space for the optimization problem. We implement the described optimization framework inside a Matlab 2022b environment.

3.3 Pareto-Frontier Evaluation

The Pareto frontier represents solutions of the multi-objective optimization defined in Eq. 15 where improvement in one objective can only be achieved at the expense of another. Within this context, the skyline operator [28] plays a crucial role in assisting our algorithm in identifying dominant and non-dominant solutions at each timestamp. The skyline operator helps extract the subset of solutions not dominated by any other solution in our multi-dimensional space. In particular, a data point is said to be in the "skyline" if no other point is better than it in all dimensions. This makes it an efficient tool for sifting through vast solution spaces to highlight those solutions that might be of particular interest due to their dominance in certain objectives. When applied to our Pareto frontier obtained from the solution of Eq. 15 at each timestamp, the skyline operator was used to refine the Pareto frontier solutions set by highlighting those solutions that stand out in particular dimensions. By focusing on skyline solutions, it is possible to have a clearer view of the trade-offs involved and prioritize solutions that align closely with strategic objectives or users' preferences. As the number of objectives of Eq. 15 is large and the solutions space is large, the skyline operator provides a more computationally efficient way to isolate dominant solutions without exhaustively comparing every possible pair of solutions. Finally, the skyline operator doesn't require any a priori knowledge about the decision maker's preferences, making it a versatile tool for our multi-objective scenarios.

4 SIMULATION STUDY

A simulation study is carried out to investigate the performance of the proposed control framework. Further, we develop an RBC, which we use to evaluate the ECMS control against a benchmark. The chosen load profile has a length of 4 h, shown in Fig. 4. It incorporates both periods of low and high load demand. While the propulsion load is shown in blue, the auxiliary loads are represented in red.

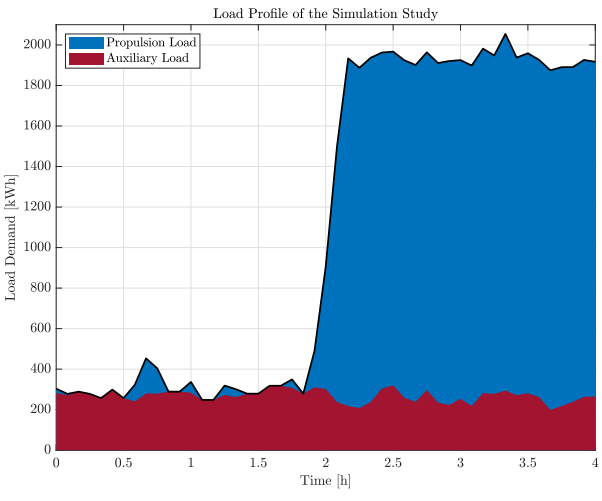

Figure 4: Load Profile

4.1 Benchmark Control

The RBC, shown as a schematic in Fig. 5, is developed with a single focus on fuel consumption while providing the requested load demand. For this, the batteries are used to buffer for fluctuation in the load and to allow a fuel-efficient operation of the engines. The engines are operated at fixed set points of the highest fuel efficiency along the propeller curve. The RBC takes the requested load demand and the current battery SoC as input values. The SoC is used to determine if the battery mode requires a change between charge and discharge. The change is initiated when the battery SoC approaches the upper or lower limit. We choose those limits to 20% and 80% SoC as a first step into battery lifetime beneficial operation. Further, we evaluate if the change in power request between the steps exceeds 350 kW. If the deviation does not exceed the limit and no change of battery mode is required, the controller keeps the previous set points. In case the set points need adjustment, the new set points are chosen according to the battery mode to either $P_{\text{Load}} \geq P_{\text{Set}}$ or $P_{\text{Load}} \leq P_{\text{Set}}$. This allows the operation of the engines at the most efficient points at all times while slowly charging or discharging the batteries.

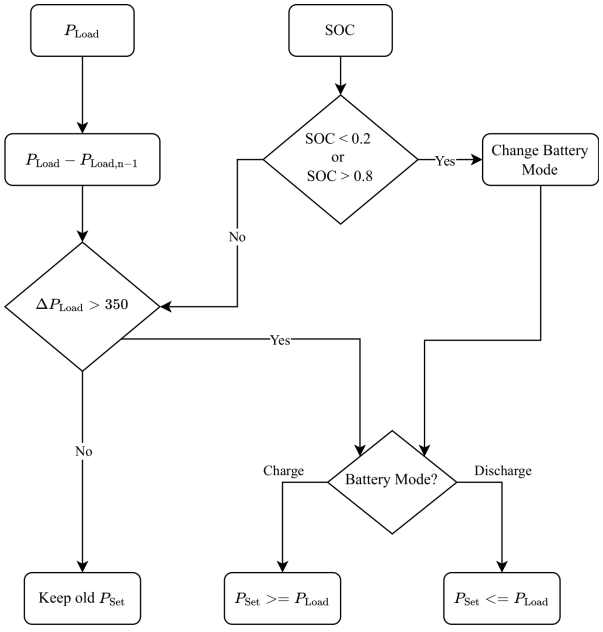

Figure 5: Decision tree of the RBC

We test the RBC on the load profile to create a benchmark. The discretization size is chosen to 5 min to allow a fair comparison with the ECMS controller. The smaller the step size of the discretization is chosen, the closer it resembles the real-world load profile in Fig. 4. In Fig. 6, the power balance at the DC bus is shown. The first subplot shows the balance between the engine and battery currents, while the second subplot compares the load demand and the provided power. The RBC is able to supply the required power demand while keeping the engines at constant power levels most of the time. The battery is used to buffer for fluctuation.

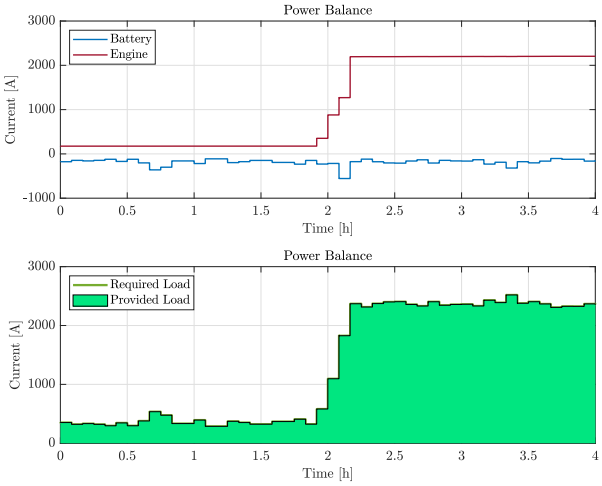

Figure 6: Current sharing and power balance with RBC. The current colors indicate the power source (engines = red, battery = blue, load = dark green, and light green = sum of produced power).

Fig. 7 shows the corresponding development of the battery SoC and the DC system voltage over the operation time. The battery behaviour is related to the left y-axis of the plot, while the voltage is depicted on the right y-axis. It is observable that the battery is slowly discharged but maintained between the upper and lower limits.

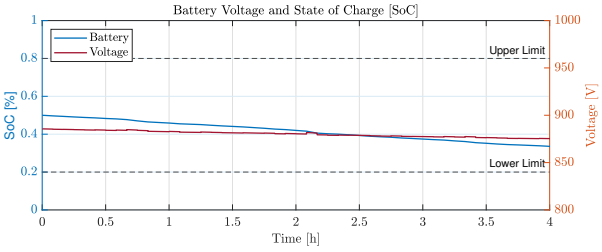

Figure 7: Battery SoC and DC system voltage using RBC. SoC is shown in blue, and Voltage in red.

In addition, the fuel consumption and the formated CO_2 and NOx emissions are calculated to compare the RBC to the ECMS in Section 5.

4.2 ECMS Control

The ECMS controller is tested with the same load profile, depicted in Fig. 4. The discretization

time step size is also chosen to 5 min. The density of diesel ρ_D is chosen according to [29] and the release rate of CO_2 from fuel r_{CO2} according to [30]. The price of diesel fuel is chosen based on an evaluation of the market as shown in Tab. 3. The equivalent pricing factor of the batteries is chosen to match the point of minimal fuel consumption of each engine to balance the power sources. Following, the equivalent factor equals the minimum SFC of the large engines when only operating those, while it corresponds to the minimum SFC of the smaller engines whenever they are involved in the power scheduling.

Some attention was spent on the choice of the penalty factor for the DoD of the battery, as a too-low factor will increase the gradient of the battery current, and a too-high factor will result in non-optimal use of the battery potential. While this factor should be investigated using a logarithmic scale to determine a good choice between flexibility and health preservation in theory, we choose a factor of $c_{\mathrm{Bat}} = 1$ in this study as a proof of concept after testing a limited amount of choices. This way, we can already showcase the performance of the ECMS control, while a full study on the effect of this parameter needs to be carried out to choose it optimally. Taking those parameters into account, the controller can determine the value of all defined objectives and minimizes the cost function Eq. 10.

Table 3: Control parameters

Parameter	Description	Value
ρ_D	Density diesel	0.838 kg/l
$r_{\mathrm{CO_2}}$	CO_2 release rate	2.7 t CO2/l
p_D	Price diesel	0.7 Euro/l
p_B	Battery equivalent cost	0.7 Euro/l
c_{Bat}	Battery penalty	1
SoC_0	Initial SoC	0.5

In our approach to determine the weights of the objectives, we employ the Pareto-Frontier combined with the skyline operator as reported in Section 3.3. This method serves as an initial step towards a deliberate a-posteriori weight selection, tailored to the end user's preferences.

5 RESULTS

In the following, we showcase the behaviour of the ECMS controller for the scenario in which we use the Pareto-Frontier combined with the skyline operator for weight selection. The power balance of the currents using the ECMS controller is shown in Fig. 8. The ECMS controller consistently meets the power demand throughout its operation. The battery serves as a buffer for load fluctuations and provides crucial support during significant power demand surges, especially during sailing.

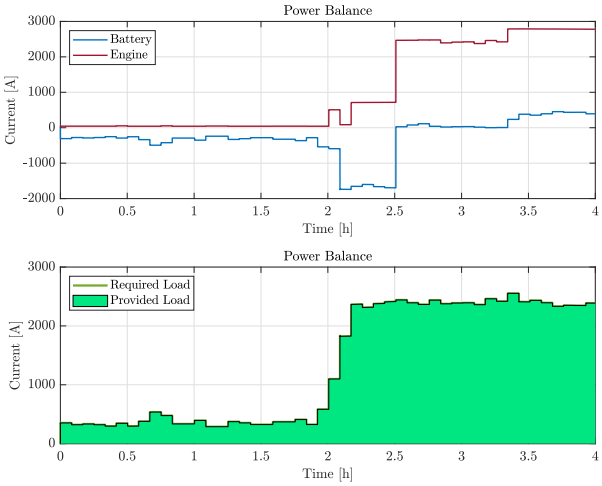

Figure 8: Current sharing and power balance with ECMS. The current colors indicate the power source (engines = red, battery = blue, load = dark green, and light green = sum of produced power).

The corresponding behaviour of the batteries and the DC system voltage is shown in Fig. 9. The SoC is represented in the left y-axis, while the voltage is connected to the right y-axis. The ECMS controller depletes the SoC fully during the large step in the load demand and slowly charges the battery again. Even though the ECMS controller breaches the lower limit of the SoC, we observe that it afterward schedules the load to charge the battery again.

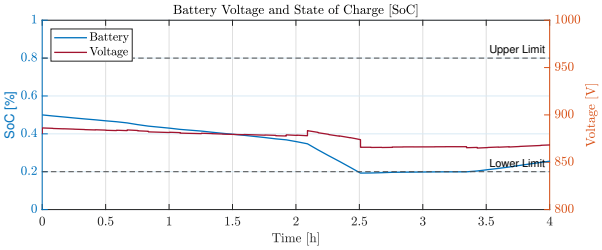

Figure 9: Battery SoC and DC system voltage using ECMS. SoC is shown in blue, and Voltage in red.

As an illustration, we assess the selected set points of the engines, as depicted in Fig. 10. In alignment with the load profile, it is evident that the controller relies solely on the smaller engines during periods of low loads. When the power demand increases drastically, the controller starts to use one of the large engines as an additional power source. Further, the controller adjusts the engine's rotational speed under operation to fully optimize the operation.

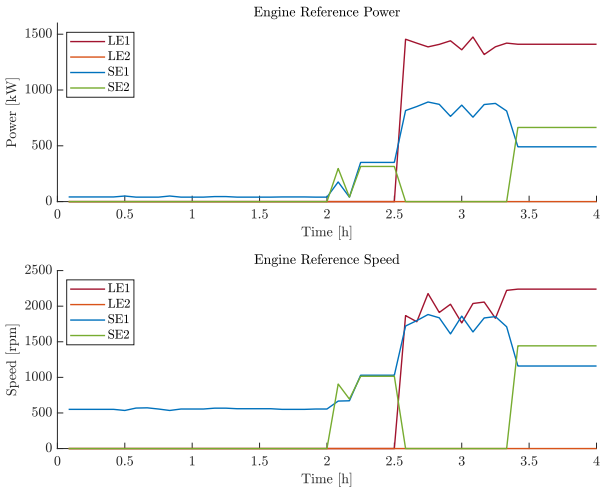

Figure 10: Power and speed reference set points for all four engines over the 4 h load profile. Each color represents a different engine.

5.1 Scenario Comparison

To further evaluate the performance of the proposed ECMS framework, we tested three scenario cases to compare with the RBC results. Two scenarios investigate edges of the Pareto-Frontier, meaning all weights besides one are set to zero, while this specific one is set to 1. The first one (SFC) is designed to singularly minimize the SFC, while the second one (NOx) only focuses on the produced NOx under operation. An overview of those scenarios' weights is presented in Tab. 4. The third scenario (Pareto) uses the Pareto-Frontier for the selection of the weights, as explained in Section 3.3.

Table 4: Scenario Design

Scenario	**SFC**	**CO_2**	**NOx**
	λ_1	λ_2	λ_3
SFC	1	0	0
NOx	0	0	1

We can evaluate the results for all three scenarios compared to the RBC. The results are presented in Tab. 5. We compare the scenarios in the aspects of consumed fuel, formatted CO_2 and NOx emissions, and the total operational cost in €. For the calculation cost, we take only the consumed fuel into account with the price assumed in Tab. 3. In addition, the percentage of deviation to the RBC is calculated for comparison and displayed in Tab. 6.

Table 5: Scenario Comparison

	Fuel	**Emission**		**Cost**
	Diesel [t]	**CO_2 [t]**	**NOx [t]**	**[€]**
RBC	0.8948	2.8829	0.0328	747.39
SFC	0.8815	2.8401	0.0223	736.33
NOx	0.9809	3.1606	0.0195	819.42
Pareto	0.9746	3.1402	0.0203	814.17

Table 6: Scenario Comparison (relative differences)

	Fuel	**Emission**		**Cost**
	Diesel [%]	**CO_2 [%]**	**NOx [%]**	**[%]**
SFC	-1.5	-1.5	-32	-1.5
NOx	+9.62	+9.6	-40	+9.6
Pareto	+8.9	+8.9	-38	+8.9

We observe a difference in the results between the three scenarios. The first scenario is the scenario that is the most similar to the setup of the RBC. Therefore, the results are relatively similar, with savings of about 1.5 % for fuel consumption, CO_2, and operational cost. This saving can be explained by a more efficient battery operation resulting in the complete discharge under operation. This result represents one edge of the Pareto-Frontier focusing only on SFC. Another edge of the Pareto-Frontier is shown in the NOx scenario. We report savings of 40 % compared to the RBC. Accompanied by that, we see an increase of about 9.6 % in fuel consumption. This is related to the fact that the most NOx efficient operating points are not equal to the fuel efficiency optima. Relating to this, the cost of the operation increases, which is basically the price paid for the saving in terms of emissions. Since the CO_2 production is linearly related to the fuel consumed, we observe an increase in CO_2 emissions alongside. The third scenario uses the Pareto-Frontier for the weight selection. We see a saving in terms of NOx formation of 38 % and a corresponding increase in fuel consumption, operational cost, and CO_2 emissions of about 8.9 %.

Evaluating the performance of the ECMS framework, we can state that the ECMS framework is able to outperform a well-designed RBC for a single-objective scenario. With the other edge of the Pareto-Frontier, we can account for maximum NOxemission savings and the corresponding price increase. Further, we showcase that a conscious decision for a compromise is possible using the Pareto-Frontier.

6 CONCLUSION

This paper presented an ECMS-based framework for multi-objective optimization of a vessel energy system. The control could fulfill the required load demand at all times while taking the fuel efficiency and emission formation of two sets of differently behaving engines into account. We implemented a Pareto-Frontier approach to allow for an a-posteriori selection of the objective weights. In three scenarios, we showed that the controller can optimize between the different optimal points for each objective based on the assigned weight in the objective function. We first tested the developed control on a $4\,\mathrm{h}$ load profile obtained from a real vessel. This allowed us to showcase the adaptation capability of the controller to adjust the performance based on the choice of objective weights. A comparison with an intelligent RBC with a focus on fuel efficiency showed the potential for up to $1.5\,\%$ savings of fuel or up to $40\,\%$ savings of NOx emissions under operation for the cases of single-objective focus.

Future work will focus on improvements in the battery handling in the control strategy. This includes more detailed research on the choice of the equivalent cost factor and the penalty factor for the DoD. Furthermore, handling delays in the system, such as engine start-up and cool-down times or set point switches, needs further study. Potential contribution can also be seen in handling the battery's health from the control perspective, which can be considered combined with a degradation model of the component. Last, further research is required on choosing the optimal objective combination from the Pareto-Frontier by implementing enhanced user selection.

ACKNOWLEDGEMENTS

This research is supported by the project MENENS, funded by the Netherlands Enterprise Agency (RVO) under the grant number MOB21012.

REFERENCES

[1] J. F. Hansen and F. Wendt, "History and State of the Art in Commercial Electric Ship Propulsion, Integrated Power Systems, and Future Trends," *Proceedings of the IEEE*, vol. 103, no. 12, pp. 2229–2242, 2015.

[2] V. Eyring, H. W. Köhler, A. Lauer, and B. Lemper, "Emissions from international shipping: 2. Impact of future technologies on scenarios until 2050," *Journal of Geophysical Research: Atmospheres*, vol. 11, no. D17, 2005.

[3] C. Nuchturee, T. Li, and H. Xia, "Energy efficiency of integrated electric propulsion for ships – A review," *Renewable and Sustainable Energy Reviews*, vol. 134, p. 110 145, 2020.

[4] P. Nema, R. K. Nema, and S. Rangnekar, "A current and future state of art development of hybrid energy system using wind and PV-solar: A review," *Renewable and Sustainable Energy Reviews*, vol. 13, no. 8, pp. 2096–2103, 2009.

[5] A. D. Korberg, S. Brynolf, M. Grahn, and I. R. Skov, "Techno-economic assessment of advanced fuels and propulsion systems in future fossil-free ships," *Renewable and Sustainable Energy Reviews*, vol. 142, p. 110 861, 2021.

[6] M. Perčić, I. Ančić, and N. Vladimir, "Life-cycle cost assessments of different power system configurations to reduce the carbon footprint in the Croatian short-sea shipping sector," *Renewable and Sustainable Energy Reviews*, vol. 131, p. 110 028, 2020.

[7] S. Atilhan, S. Park, M. M. El-Halwagi, M. Atilhan, M. Moore, and R. B. Nielsen, "Green hydrogen as an alternative fuel for the shipping industry," *Current Opinion in Chemical Engineering*, vol. 31, p. 100 668, 2021.

[8] M. Prussi, N. Scarlat, M. Acciaro, and V. Kosmas, "Potential and limiting factors in the use of alternative fuels in the European maritime sector," *Journal of Cleaner Production*, vol. 291, p. 125 849, 2021.

[9] F. D. Kanellos, A. Anvari-Moghaddam, and J. M. Guerrero, "A cost-effective and emission-aware power management system for ships with integrated full electric propulsion," *Electric Power Systems Research*, vol. 150, pp. 63–75, Sep. 2017, ISSN: 0378-7796. (visited on 08/31/2022).

[10] F. D. Kanellos, "Optimal Power Management With GHG Emissions Limitation in All-Electric Ship Power Systems Comprising Energy Storage Systems," *IEEE Transactions on Power Systems*, vol. 29, no. 1, pp. 330–339, Jan. 2014, ISSN: 1558-0679.

[11] D. Gao, X. Wang, T. Wang, Y. Wang, and X. Xu, "An Energy Optimization Strategy for Hybrid Power Ships under Load Uncertainty Based on Load Power Prediction and Improved NSGA-II Algorithm," *Energies*, vol. 11, no. 7, p. 1699, Jul. 2018, ISSN: 1996-1073. (visited on 01/20/2023).

[12] S. Fang, Y. Xu, Z. Li, T. Zhao, and H. Wang, "Two-Step Multi-Objective Management of Hybrid Energy Storage System in All-Electric Ship Microgrids," *IEEE Transactions on Vehicular Technology*, vol. 68, no. 4, 2019.

[13] C. Tsoumpris and G. Theotokatos, "A health-aware energy management strategy for autonomous ships power plants operation," *Transportation Research Procedia*, p. 8, 2019.

[14] M. Banaei, M. Rafiei, J. Boudjadar, and M.-H. Khooban, "A Comparative Analysis of Optimal

Operation Scenarios in Hybrid Emission-Free Ferry Ships," *IEEE Transactions on Transportation Electrification*, vol. 6, no. 1, pp. 318–333, Mar. 2020, ISSN: 2332-7782.

[15] K. Hein, Y. Xu, G. Wilson, and A. K. Gupta, "Coordinated Optimal Voyage Planning and Energy Management of All-Electric Ship With Hybrid Energy Storage System," *IEEE Transactions on Power Systems*, vol. 36, no. 3, pp. 2355–2365, May 2021, ISSN: 1558-0679.

[16] K. Hein, X. Yan, and G. Wilson, "Multi-Objective Optimal Scheduling of a Hybrid Ferry with Shore-to-Ship Power Supply Considering Energy Storage Degradation," *Electronics*, vol. 9, no. 5, p. 849, May 2020, ISSN: 2079-9292. (visited on 08/31/2022).

[17] H. Li, A. Ravey, A. N'Diaye, and A. Djerdir, "A novel equivalent consumption minimization strategy for hybrid electric vehicle powered by fuel cell, battery and supercapacitor," *Journal of Power Sources*, vol. 395, pp. 262–270, 2018.

[18] M. Kalikatzarakis, R. D. Geertsma, E. J. Boonen, K. Visser, and R. R. Negenborn, "Ship energy management for hybrid propulsion and power supply with shore charging," *Control Engineering Practice*, vol. 76, pp. 133–154, 2018.

[19] O. Tremblay, L.-A. Dessaint, and A.-I. Dekkiche, "A Generic Battery Model for the Dynamic Simulation of Hybrid Electric Vehicles," in *2007 IEEE Vehicle Power and Propulsion Conference*, 2007.

[20] F. Rosero, N. Fonseca, J.-M. López, and J. Casanova, "Real-world fuel efficiency and emissions from an urban diesel bus engine under transient operating conditions," *Applied Energy*, vol. 261, p. 114 442, Mar. 2020, ISSN: 0306-2619. (visited on 05/24/2023).

[21] R. D. Geertsma, R. R. Negenborn, K. Visser, and J. J. Hopman, "Design and control of hybrid power and propulsion systems for smart ships: A review of developments," *Applied Energy*, vol. 194, pp. 30–54, 2017.

[22] M. J. Kochenderfer and T. A. Wheeler, *Algorithms for decision making*. Mit Press, 2022.

[23] D. Wolpert and W. Macready, "No free lunch theorems for optimization," *IEEE Transactions on Evolutionary Computation*, vol. 1, no. 1, pp. 67–82, Apr. 1997, ISSN: 1941-0026.

[24] P. T. Boggs and J. W. Tolle, "Sequential quadratic programming," *Acta numerica*, vol. 4, pp. 1–51, 1995.

[25] Z. Khalik, G. Padilla, T. Romijn, and M. Donkers, "Vehicle energy management with ecodriving: A sequential quadratic programming approach with dual decomposition," in *2018 Annual American Control Conference (ACC)*, IEEE, 2018, pp. 4002–4007.

[26] S. Mennen, F. P. Willems, and M. Donkers, "A sequential quadratic programming approach to combined energy and emission management of a heavy-duty parallel-hybrid vehicle," *IFAC-PapersOnLine*, vol. 55, no. 24, pp. 335–341, 2022.

[27] R. Martí, "Multi-start methods," in *Handbook of Metaheuristics*, 2003.

[28] S. Borzsony, D. Kossmann, and K. Stocker, "The Skyline operator," in *Proceedings 17th International Conference on Data Engineering*, Apr. 2001, pp. 421–430.

[29] F. Murphy, K. McDonnell, E. Butler, and G. Devlin, "The evaluation of viscosity and density of blends of Cyn-diesel pyrolysis fuel with conventional diesel fuel in relation to compliance with fuel specifications EN 590:2009," *Fuel*, vol. 91, no. 1, pp. 112–118, 2012.

[30] A. Q. Jakhrani, A. R. H. Rigit, A.-K. Othman, S. R. Samo, and S. A. Kamboh, "Estimation of carbon footprints from diesel generator emissions," in *2012 International Conference on Green and Ubiquitous Technology*, 2012, pp. 78–81.